

Article

Precipitation Strengthening in Ni–Cu Alloys Fabricated Using Wire Arc Additive Manufacturing Technology

Olexandra Marenych ^{1,2}, Andrii Kostryzhev ¹, Chen Shen ^{1,2}, Zengxi Pan ^{1,2,*}, Huijun Li ^{1,2} and Stephen van Duin ^{1,2}

¹ School of Mechanical, Materials, Mechatronics and Biomedical Engineering, University of Wollongong, Northfields Avenue, Wollongong, NSW 2500, Australia; om753@uowmail.edu.au (O.M.); andrii@uow.edu.au (A.K.); cshen@uow.edu.au (C.S.); huijun@uow.edu.au (H.L.); svanduin@uow.edu.au (S.v.D.)

² Defence Materials Technology Centre, Hawthorn, VIC 3122, Australia

* Correspondence: zengxi@uow.edu.au; Tel.: +61-02-4221-5498

Received: 18 December 2018; Accepted: 18 January 2019; Published: 21 January 2019



Abstract: Two Ni–Cu alloys, Monel K500 and FM60, with various contents of Ti, Mn, Al, Fe and C were deposited in the form of plates on a metal base plate using wire arc additive manufacturing technology. Three deposition speeds have been applied: 300, 400 and 500 mm/min. To modify the as-welded microstructure and properties, the deposited walls/plates have been subjected to two heat treatment procedures: annealing at 1100 °C for 15 min, slow cooling to 610 °C, ageing at this temperature for 8 h and either (i) air cooling to room temperature or (ii) slow cooling to 480 °C, ageing at this temperature for 8 h and air cooling to room temperature. The microstructure characterisation and mechanical properties testing have been conducted for each of the 18 chemistry/processing conditions. The dependences of the precipitate's parameters (size, number density and chemistry), mechanical properties and wear resistance on the alloy composition, deposition speed and heat treatment have been obtained. In Monel K500, the precipitates were mainly of the TiC/TiCN type, and in FM60, they were of the MnS and TiAlMgO types. Monel K500 has shown higher hardness, strength, toughness and wear resistance in all studied conditions. Ageing at 610 °C improved properties in both alloys following the precipitation of new particles. Ageing at 480 °C could result in a properties loss if the particle coarsening (decrease in number density) took place.

Keywords: Ni–Cu alloys; wire arc additive manufacturing; microstructure characterisation; mechanical properties; wear resistance

1. Introduction

Ni-base alloys are recognised for their superior resistance to many corrosive environments and good mechanical properties. These single-phase alloys retain an austenitic matrix from solidification to subzero temperatures. Thus, they are widely used in many applications, particularly, in the marine industry to produce valves, pumps and propeller shafts, marine fixtures and fasteners and electrical and electronic components. The 70Ni–30Cu alloy system, also known as the Monel family, has a high tolerance for alloying elements in solid solutions. This resulted in the development of Monel alloys with multiple alloying additions providing a wide variety of properties [1]. Cu, Co, Fe, Al and Ti are effective solid solution strengtheners of the Ni matrix [2,3]. The addition of Al promotes the formation of a surface oxide layer, which provides corrosion resistance in many environments [4]. Monel 400 can be strengthened only by C, Mn and Si in solid solutions, since any additional heat treatment will cause the alloy's mechanical properties to decrease. Increased amounts of Ti (up to 0.85 wt.%) led to the

appearance of the first age-hardenable Ni-alloy, known today as Monel K500 [5]. Solution annealing and ageing of this alloy results in precipitation strengthening with γ' -Ni₃(Al,Ti) and TiC particles.

Wire arc additive manufacturing (WAAM) is a rapidly developing low-cost technology. It uses an electric arc as a heat source and a wire, rather than powder, as feedstock. One of the advantages of WAAM technology is the absence of a technically complex and expensive powder bed system. WAAM can be implemented using off-the-shelf welding equipment. Apart from the manufacturing of new components, WAAM can also be used for maintenance and repair operations.

Recent publications reported successful application of WAAM for making Ti-base [6,7], Fe-base [8,9], Al-base [10], Cu-base [11] and Ni–Cr-base [12,13] alloy components. However, detailed investigation of the effect of WAAM processing parameters on microstructure and mechanical properties of the components has not been conducted. WAAM of Ni–Cu alloys has not been previously reported. In this work, we present a first-ever study of the effect of heat treatment on the microstructure, mechanical properties and wear resistance of Ni–Cu alloys obtained using WAAM technology. The grain structure and particle precipitation (chemistry and size distribution) have been shown to significantly vary with alloy composition and heat treatment. The microstructure-properties relationship for the studied Ni–Cu alloys is discussed.

2. Materials and Experimental Techniques

Two welding consumables of varying chemical composition (Table 1), a commercially produced Monel K500 wire with diameter 1.0 mm and ERNiCu-7 (FM60) wire with diameter 1.2 mm, were used in this study to investigate the effects of alloy composition and heat treatment schedule on microstructure and mechanical properties. A Monel K500 hot-rolled plate of 8 mm thickness was used as the substrate on which the wires were deposited and as a reference for the mechanical properties.

Table 1. The chemical compositions of Monel K500 and FM60 used in the study (wt.%).

Alloy	Ni	Mn	Fe	Si	Al	Ti	C	S	P	Cu
Monel K500	68.3	0.8	1.29	0.17	3.0	0.5	0.088	0.003	0.003	bal.
FM60	67.2	3.2	0.08	0.07	0.2	1.5	0.004	0.014	0.003	bal.

A robotic welding system installed at the University of Wollongong was used to produce the samples for this study. The wire deposition was carried out by the cold metal transfer (CMT) method using an ABB 1400 robot (ABB group, Zurich, Switzerland) with a Fronius CMT welder in the flat position. CMT technology is a modified gas metal arc welding (GMAW) process with controlled droplet detachment in short circuit transfer mode. When a short circuit occurs, the welding current drops and the filler wire starts to retract. At this moment, one droplet of metal is detached into the molten weld pool, then the filler wire moves forward and the cycle is repeated. This technology facilitates a controlled droplet detachment and gives a clean, spatter-free material transfer. Welding grade argon (99.995% purity) was used for shielding with 10 L/min gas flow rate. A preliminary research (not shown here) was conducted in order to evaluate the range of the welding parameters, which would be optimal for the studied alloys and a chosen deposition technology. Both alloys have been deposited at one wire feed rate of 8.3 m/min and three torch travel speeds: 300, 400 and 500 mm/min. The 55 mm wide and 180 mm long plates have been produced via depositing one pass of material next to the other (Figure 1). Fewer passes were required for a slower travel speed and more passes for a faster travel speed. Namely, 11, 14 and 16 passes were required for Monel K500, and 10, 11 and 15 passes were required for FM60, deposited at travel speeds of 300, 400 and 500 mm/min, respectively. The average heat input for 300, 400 and 500 mm/min travel speeds were calculated to be 550, 425 and 340 J/mm, respectively, in Monel K500 and 370, 280 and 220 J/mm, respectively, in FM60. Samples for mechanical testing were prepared by wire cutting.

In order to investigate the effect of heat treatment on microstructure and properties, the following heat treatment schedules have been applied for both alloy depositions and the hot-rolled plate: heating to the annealing temperature of 1100 °C with the rate of 10 °C min^{−1}, holding at this temperature for 15 min and either (i) slow cooling to 610 °C, holding for 8 h at this temperature and air cooling to room temperature, or (ii) slow cooling to 610 °C, holding for 8 h, slow cooling to 480 °C and holding for 8 h followed by air cooling to room temperature (Figure 2). Heat treatment was performed using a KTL1400 tube furnace (Across International, Livingston, NJ, USA). The samples were treated in vacuum.

Sample preparation for microscopy included mounting in Polyfast resin, polishing on Struers Tegramin automatic polisher (Struers, Ballerup, Denmark) to 1 µm finish and etching with ferric chloride solution. Optical microscopy was carried out by using a Leica M205A stereo microscope (Leica, Wetzlar, Germany) and Leica DM 6000M microscope equipped with Leica Application Suite (LAS) 4.0.0 image processing software. Scanning electron microscopy was conducted using a JEOL7001F FEG scanning electron microscope (JEOL, Akishima, Tokyo, Japan) (SEM) operating at 15 kV. The energy dispersive X-ray spectroscopy (EDS) semi-quantitative point analysis of precipitates and the element distribution mapping were carried out using an AZtec 2.0 Oxford SEM EDS system (Oxford Instruments, Abingdon, UK). For the determination of particles' composition, size and number density, 150–200 particles were analysed for each studied condition. The element distribution mapping was carried out 2 to 3 times from various locations for each studied condition.

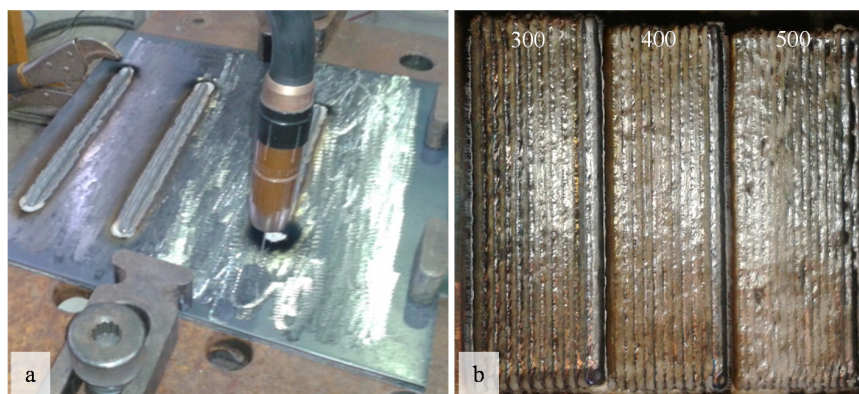


Figure 1. The deposition of FM60 plates at three travel speeds of 300, 400 and 500 mm/min: (a) the beginning of deposition process and (b) fabricated plates.

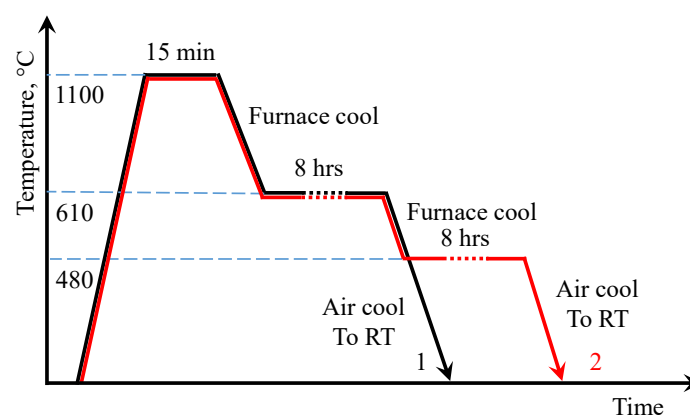


Figure 2. A schematic illustration of the heat treatment procedure.

Tensile tests were performed on an MTS Landmark servohydraulic testing machine (MTS Systems Corporation, Eden Prairie, MN USA), model 370.02. Subsize flat dog-bone type samples of 10 mm gage length, 2 mm width and 1.5 mm thickness were cut from the deposited plates, perpendicular

to the direction of material deposition. For each condition, 3 to 4 samples were tested at ambient temperature at a strain rate of $1 \times 10^{-3} \text{ s}^{-1}$.

Microhardness testing was conducted on Struers DuraScan Vickers hardness tester with a 0.5 kg load. Up to ten indentations were performed for each sample, with a distance of approximately ten times the length of the indent diagonals to ensure that the results were not contaminated by work hardening from previous indentations. The indentation dwell time was 14 s according to the standard ASTM E384.

The wear testing was carried out on a CETR tribological station (Bruker, Billerica, Massachusetts, USA) utilising a pin-on-disk type of test according to the standard ASTM G 99–95a. The testing was conducted at ambient temperature without lubrication. The samples, 50 mm in diameter discs, were cut from the deposited plates, grinded to flat surface and polished with silicon carbide paper 2000 (10 micron). The pin with a spherical tip made of wear resistant steel with a martensitic microstructure was used as a contact pair. Each sample underwent 3 successive testing cycles with 750 s of total sample-disk interaction time, a track diameter of 30 mm, a velocity of 0.758 m/s (500 rpm) and a total path length of 600 m. One test cycle included vertical loading of the pin to 15 N load (in compression against the sample disk) and rotation of the disk for 250 s. The wear resistance was assessed via the sample mass loss measured after each cycle (i.e., after 250, 500 and 750 s of testing time) and the final width and depth of the wear track. The sample mass was measured on fine analytical scales Nuweight AS 310.R2 (Nuweigh, NSW, Australia) with an accuracy of 0.0001 gram. The wear track surface roughness was assessed on a ContourGT-K 3D Optical Microscope (Bruker, Billerica, MA, USA) equipped with the Vision 64 software. The measurements were performed in the voltage source inverter (VSI) mode; green light was used for illumination. Four Y-profile curves from two topological maps were analysed to evaluate the mean maximum roughness depth value.

3. Results

3.1. Microstructure Characterisation

Optical microscopy revealed a single-phase microstructure in both alloys (Figure 3). In the as-weld condition, minor Cu segregation was observed, although other elements did not segregate significantly (Figure 4a–f). The Cu segregation was significantly reduced by annealing at 1100 °C for 15 min (Figure 4g–i). In the as-weld condition, the secondary dendrite arm spacing (SDAS) was measured to be 4–12 µm in both alloys. In Monel K500, SDAS decreased with an increase in deposition speed, from 6–12 µm for 300 mm/min to 5–10 µm for 400 mm/min to 4–8 µm for 500 mm/min. However, in FM60, no dependence of SDAS on deposition speed was observed. In both alloys, SDAS increased following annealing and ageing at 610 °C; however the growth was larger in FM60 (up to 10–18 µm) compared to Monel K500 (up to 6–14 µm). No significant grain growth occurred during the second ageing.

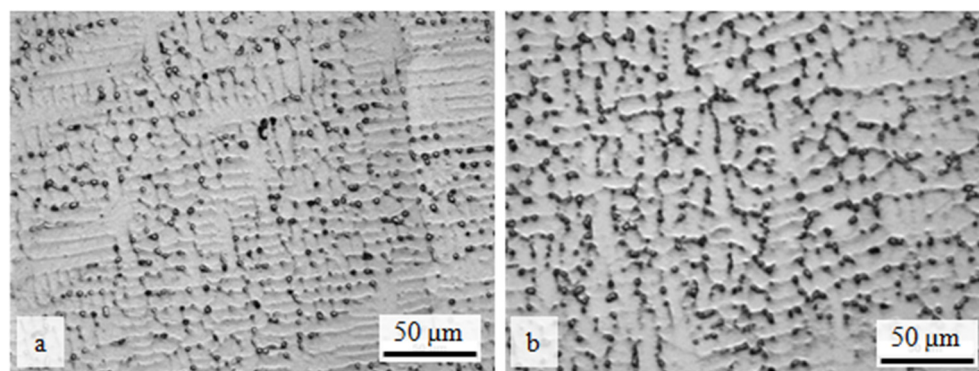


Figure 3. The optical images of the dendritic structure in the as-weld condition in (a) Monel K500 and (b) FM60 (travel speed of 400 mm/min).

SEM studies have shown <700 nm precipitates in Monel K500 and <1000 nm in FM60 (Figure 5). The particle chemistry and size distribution varied with alloy composition and heat treatment. In Monel K500 the particles were mainly TiC, TiCN, MnS, MnSMgO and MnSAlMgO (Table 2), and in FM60 the particles were mainly MnS, MnSAlMgO and TiAlMgO (Table 3).

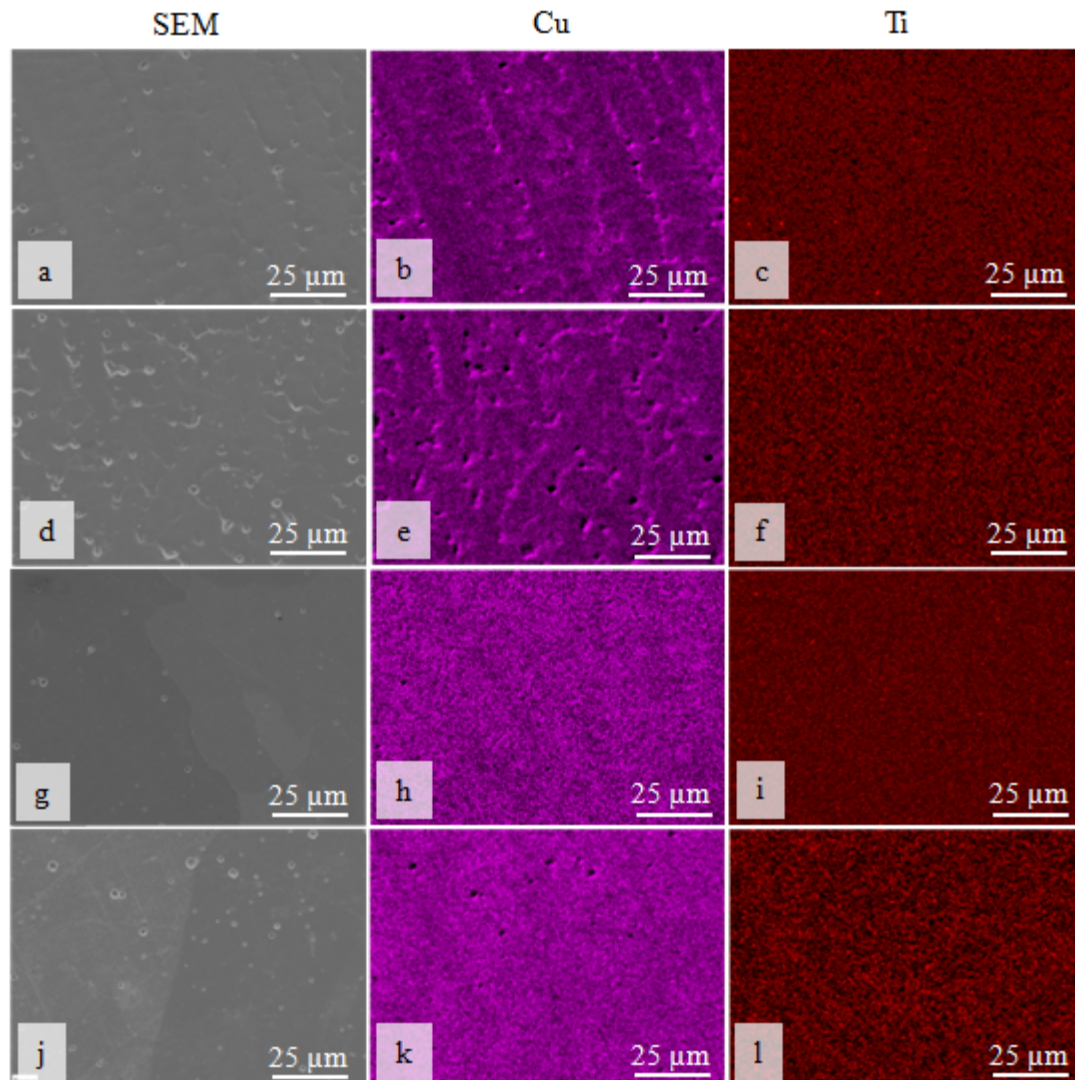


Figure 4. Representative SEM images of the microstructure in (a,g) Monel K500 and (d,j) FM60, and energy dispersive X-ray spectroscopy (EDS) maps showing Cu segregation in as-weld (b) Monel K500 and (e) FM60, absence of Cu segregation in annealed (h) Monel K500 and (k) FM60, absence of Ti segregation in as-weld (c) Monel K500 and (f) FM60 and absence of Ti segregation in annealed (i) Monel K500 and (l) FM60 (travel speed of 500 mm/min).

In the as-weld condition, the majority of particles were Ti-rich (64%–72%) in Monel K500 and Mn-rich (66%–80%) in FM60. The particle number density was on average twice as high in FM60. The particle number density decreased with an increase in deposition speed from $3.6 \times 10^{-3} \mu\text{m}^{-2}$ for 300 mm/min to $3.1 \times 10^{-3} \mu\text{m}^{-2}$ for 400 mm/min to $2.6 \times 10^{-3} \mu\text{m}^{-2}$ for 500 mm/min in Monel K500 and from $11.4 \times 10^{-3} \mu\text{m}^{-2}$ for 300 mm/min to $7.2 \times 10^{-3} \mu\text{m}^{-2}$ for 400 mm/min to $4.7 \times 10^{-3} \mu\text{m}^{-2}$ for 500 mm/min in FM60.

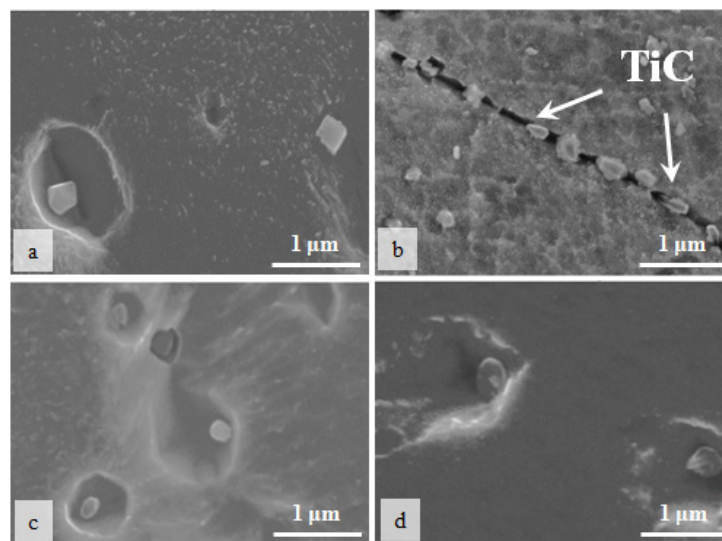


Figure 5. SEM images of the precipitates in (a,b) Monel K500 and (c,d) FM60 in (a,c) as-weld and (b,d) aged at 610 °C conditions (travel speed of 500 mm/min).

After annealing and ageing at 610 °C, the particle number density increased by 240–290 times in Monel K500 and only up to 70% in FM60. This coincided with a 4–6 times decrease in the average particle size in Monel K500 and only a 10%–60% decrease in FM60. After annealing and ageing almost all the particles in Monel were Ti-rich (Figure 6a,b). Although in the as-weld condition, around 70% of particles were Ti-rich. In contrast, in FM60, the particle chemistry did not vary significantly in the aged condition compared to the as-weld (Figure 6c,d). In Monel K500, the dependence of the particle parameters on deposition speed, observed in the as-weld conditions, disappeared after annealing and ageing. Although in FM60, the dependence on deposition speed (a decrease in the particle number density with an increase in speed) remained after annealing and ageing. All these indicate a stronger effect of annealing and ageing on particle precipitation in Monel K500, compared to FM60: Ti-rich particles broadly precipitated in Monel K500 during ageing, although in FM60, this process was much slower.

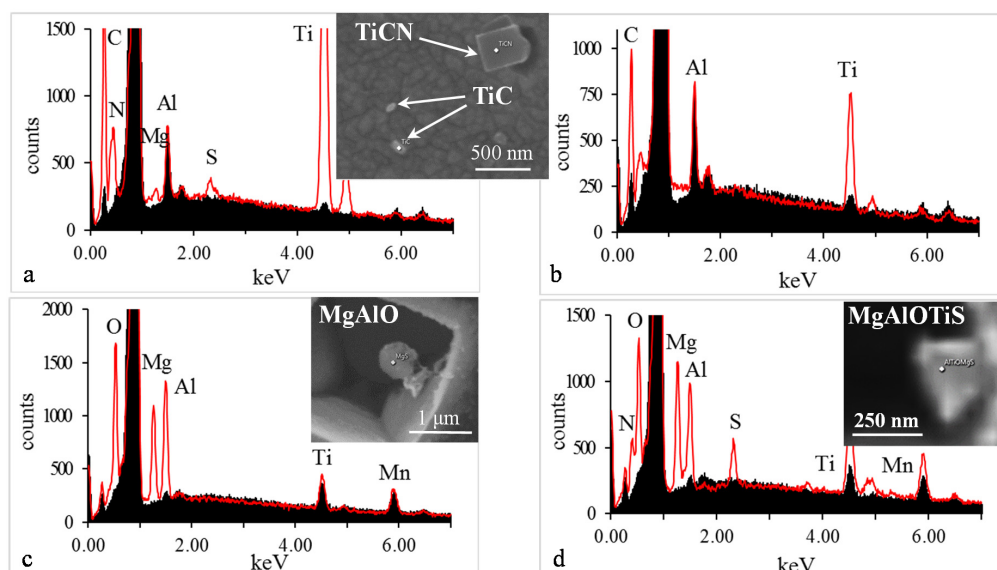


Figure 6. EDS spectra showing the chemical composition of (a) TiC and (b) TiCN particles in Monel K500 aged at 610 °C and (c) MgAlO and (d) AlTiOMgS in FM60 aged at 610 °C (the travel speed of 500 mm/min). The matrix spectrum is shown in black; the particle spectrum is shown in red.

During the second ageing at 480 °C, following annealing and ageing at 610 °C, the particle coarsening accompanied by a decrease in the particle number density took place in both alloys. However, this was more pronounced in Monel K500 (up to a 1.7 times increase in the average particle size and up to a 2 times decrease in the particle number density with respect to the condition after first ageing) compared to FM60 (up to a 10% increase in the average particle size, which could be within the experimental error, and up to a 40% decrease in the particle number density). In Monel K500, no significant variation in the particle chemistry was observed with the second ageing; all the particles were Ti-rich. In FM60, the relative amount of Mn-rich particles increased after the second ageing.

Table 2. The microstructural parameters and mechanical properties variation with heat treatment in Monel K500.

Heat Treatment Condition		Particles (SEM Size Range)			Mechanical Properties						
		ND * $\times 10^{-3} \mu\text{m}^{-2}$	Size, nm	Chemistry, %	HV	YS, MPa	UTS, MPa	El, %	MPa-%	Wear Mass Loss, g	Wear Track Width, mm Max. Depth, μm
As-weld	300	3.6	437 \pm 150	72 Ti-rich 28 Mn-rich	144	170 \pm 5	430 \pm 15	47 \pm 2	14,100	0.0896	2.101 106
	400	3.1	448 \pm 140	69 Ti-rich 31 Mn-rich	141	165 \pm 10	410 \pm 10	51 \pm 3	14,662	0.0662	2.124 100
	500	2.6	331 \pm 160	64 Ti-rich 36 Mn-rich	148	160 \pm 5	408 \pm 15	50 \pm 1	14,200	0.0685	2.160 75
Age at 610	300	865	90 \pm 50	100 Ti-rich	256	250 \pm 4	522 \pm 25	39 \pm 1	15,054	0.0758	1.923 106
	400	898	75 \pm 45	100 Ti-rich	255	300 \pm 3	615 \pm 20	37 \pm 1	16,928	0.0601	2.057 90
	500	692	85 \pm 47	100 Ti-rich	262	290 \pm 4	609 \pm 15	32 \pm 1	14,384	0.0556	2.190 47
Age at 610 + 480	300	448	160 \pm 74	100 Ti-rich	259	320 \pm 3	536 \pm 5	12 \pm 1	5,136	0.0748	2.020 82
	400	667	90 \pm 50	100 Ti-rich	236	250 \pm 5	563 \pm 5	34 \pm 4	13,821	0.0625	2.105 48
	500	641	95 \pm 45	100 Ti-rich	265	280 \pm 3	622 \pm 20	31 \pm 1	13,981	0.0589	2.270 43

ND * is the number density of particles.

Table 3. The microstructural parameters and mechanical properties variation with heat treatment in FM60.

Heat Treatment Condition		Particles (SEM Size Range)			Mechanical Properties						
		ND $\times 10^{-3} \mu\text{m}^{-2}$	Size, nm	Chemistry, %	HV	YS, MPa	UTS, MPa	El, %	MPa-%	Wear Mass Loss, g	Wear Track Width, mm Max. Depth, μm
As-weld	300	11.4	311 \pm 170	67Mn-rich 33TiAl-rich	131	146 \pm 3	356 \pm 10	48 \pm 3	12,048	0.0902	2.234 132
	400	7.2	392 \pm 150	66Mn-rich 34TiAl-rich	132	149 \pm 5	361 \pm 20	47 \pm 1	11,985	0.0722	2.240 124
	500	4.7	388 \pm 160	80Mn-rich 20TiAl-rich	134	160 \pm 4	375 \pm 5	48 \pm 2	12,840	0.0744	2.379 95
Age at 610	300	12.7	278 \pm 90	52Mn-rich 48TiAl-rich	163	160 \pm 3	397 \pm 5	41 \pm 1	10,804	0.0689	1.730 107
	400	8.5	274 \pm 110	50Mn-rich 50TiAl-rich	164	155 \pm 5	410 \pm 10	43 \pm 1	11,718	0.0639	2.085 85
	500	8.1	236 \pm 95	55Mn-rich 45TiAl-rich	162	205 \pm 3	428 \pm 20	36 \pm 3	11,034	0.0587	2.105 65
Age at 610 + 480	300	9.2	285 \pm 100	61Mn-rich 39TiAl-rich	139	115 \pm 4	358 \pm 10	48 \pm 2	11,160	0.0734	2.200 94
	400	8.9	288 \pm 97	70Mn-rich 30TiAl-rich	192	170 \pm 3	490 \pm 20	39 \pm 1	12,870	0.0680	2.208 86
	500	7.7	261 \pm 95	62Mn-rich 38TiAl-rich	173	190 \pm 5	428 \pm 20	40 \pm 2	11,760	0.0602	2.220 79

3.2. Tensile Properties

The yield stress (YS) and ultimate tensile strength (UTS) were higher in Monel K500 than in FM60 for all studied conditions, although this discrepancy varied with heat treatment (Figure 7, Tables 2 and 3). In the as-weld condition, YS and UTS were 16–24 MPa (depending on deposition speed) and 33–74 MPa, respectively, higher in Monel K500. After annealing and ageing at 610 °C, the YS and UTS were 90–145 MPa and 125–205 MPa, respectively, higher in Monel K500. These indicate a higher strength growth with ageing at 610 °C in Monel K500 compared to FM60: in Monel K500, the YS and UTS increased by 80–130 MPa and 92–205 MPa, respectively; however, in FM60, the YS and UTS increased by only 6–45 MPa and 42–53 MPa, respectively. With the second ageing at 480 °C, following annealing and ageing at 610 °C, the YS and UTS could decrease in both alloys by up to 45 MPa. In the as-weld condition, the elongation to failure was slightly higher in Monel K500 (50–51%) compared to FM60 (47–48%). However, after ageing, the elongation in Monel K500 decreased faster than in FM60 and became lower than in FM60.

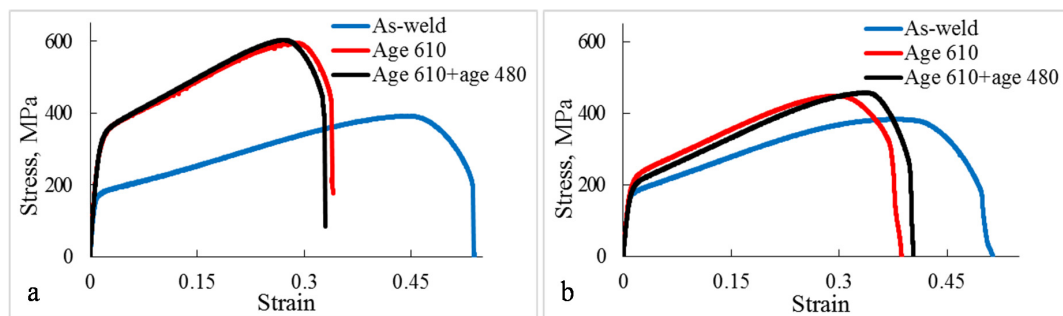


Figure 7. The stress–strain curves of (a) Monel K500 and (b) FM60 for the torch travel speed of 500 mm/min and various heat treatment conditions.

3.3. Hardness, Toughness and Wear Resistance

Hardness in Monel K500 was higher than in FM60 for all studied conditions (Tables 2 and 3). However, the difference was minor (9–14 HV) in the as-weld condition and increased significantly (90–100 HV) after annealing and ageing at 610 °C. This coincides with a larger hardness response of Monel K500 to ageing: as a result of annealing and ageing at 610 °C, hardness in Monel K500 increased by 112–114 HV, although in FM60 it increased by only 28–32 HV. The second ageing at 480 °C did not improve the hardness of Monel K500. However, in FM60, the hardness could increase by up to 28 HV as a result of the second ageing. A decrease in hardness following the second ageing was also observed (for 400 mm/min deposition speed in Monel K500 and for 300 mm/min speed in FM60).

Toughness was assessed via the calculation of the area under the stress–strain curves. The shape under the stress–strain curves was approximated by a trapezoid with the area calculated as $0.5(YS + UTS) \cdot \text{elongation}$. For such a calculation method, the toughness units were MPa·%. Toughness in Monel K500 was higher than in FM60 for all studied conditions (except for 300 mm/min deposition speed aged at 480 °C, which showed abnormally low elongation in Monel K500). In Monel K500, toughness increased after annealing and ageing at 610 °C by up to 15%, which corresponds to a significant increase in strength, and decreased after the second ageing at 480 °C by up to 8%, due to a decrease in elongation. In FM60, the opposite trend was observed: toughness decreased after annealing and ageing at 610 °C by up to 15% and increased after the second ageing at 480 °C by up to 10%.

The wear resistance was higher (sample mass loss lower) in Monel K500 for almost all studied conditions. After annealing and ageing at 610 °C, the wear resistance increased by up to 16% in Monel K500 and up to 24% in FM60. These correspond to an increase in hardness in both alloys and some increase in toughness in Monel K500. After the second ageing at 480 °C, the wear resistance slightly (by up to 6%) decreased in both alloys. In Monel K500, this coincided with a decrease in toughness. Although in FM60, no direct correlation with hardness and toughness was observed. Imaging of the wear surfaces (Figure 8) and measurements of the wear track roughness (Figure 9) supported the mass loss data. In the as-weld condition, both alloys exhibited quite rough wear surfaces with numerous debris and deep wear track grooves, indicating pronounced plastic deformation, fatigue and ductile fracture during the wear process (Figure 8a,c and Figure 9a,d). Although, the wear track width was 6–10% narrower and the depth was 25% shallower for Monel K500 than for FM60, meaning more a difficult penetration of the pin into the Monel K500 disk surface. This corresponds to a lower mass loss measured for Monel K500 and contributes to the overall conclusion that the wear resistance of as-weld Monel K500 was higher. After annealing followed by ageing at 610 °C, the wear track roughness decreased for both alloys (Figure 8b,d and Figure 9b,e). In particular, the track depth decrease reached 65% in both alloys, which corresponds to a decrease in mass loss for both alloys. This can be correlated to an increase in hardness for both alloys with the ageing and indicates a transition towards a more sliding abrasion type of wear from a more fatigue type for the as-weld condition. After the second ageing at 480 °C, the wear track width increased for both alloys, although the track depth mainly decreased. This corresponds to an increase in mass loss and supports a decrease in wear resistance with the second ageing.

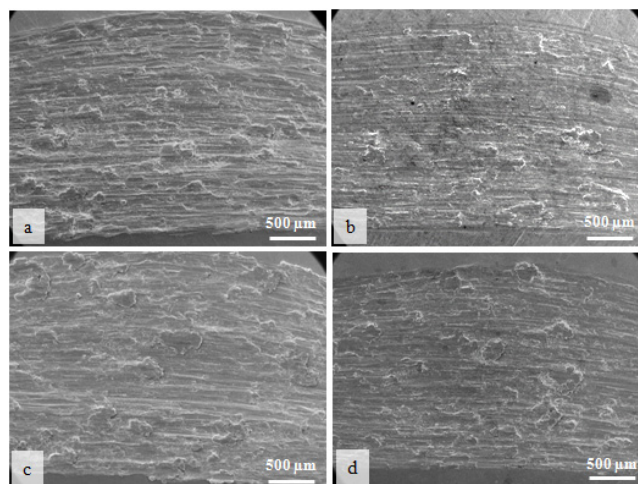


Figure 8. SEM images of the wear tracks for Monel K500 in (a) as-weld and (b) annealed and aged at 610 °C conditions and for FM60 in (c) as-weld and (d) annealed and aged at 610 °C conditions for the torch travel speed of 500 mm/min.

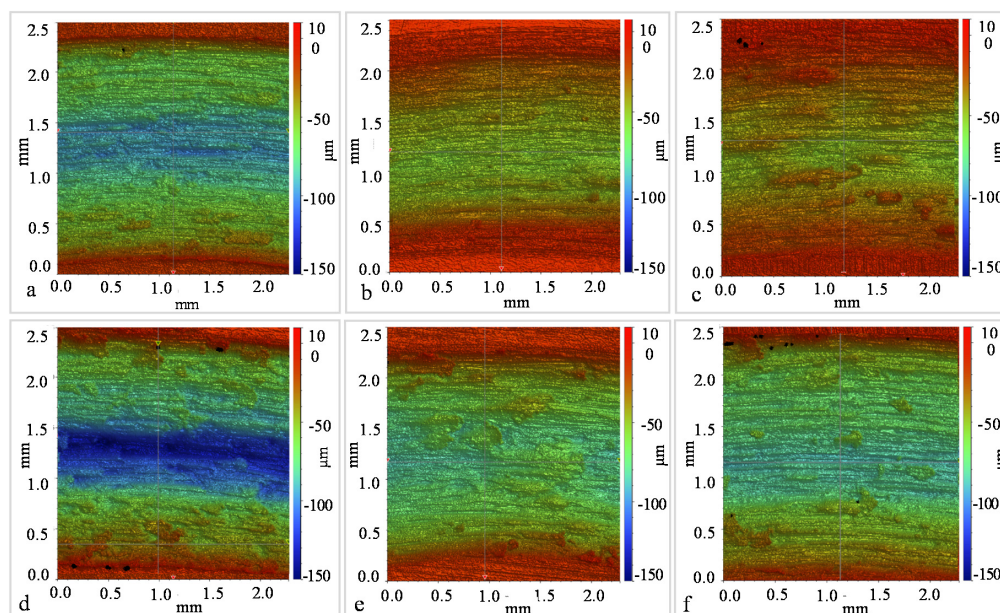


Figure 9. Surface roughness maps of the wear tracks for Monel K500 in (a) as-weld, (b) annealed and aged at 610 °C and (c) annealed and aged at 610 °C + 480 °C conditions and for FM60 in (d) as-weld, (e) annealed and aged at 610 °C and (f) annealed and aged at 610 °C + 480 °C conditions (travel speed of 500 mm/min).

3.4. Mechanical Properties of Hot Rolled Monel K500 Plate

Mechanical properties of the Monel K500 hot-rolled plate are presented in Figure 10 and Table 4. As can be seen, the age hardening heat treatment at 610 °C has led to the increased strength, hardness and wear resistance compared to the annealed condition, although the elongation to failure decreased after ageing by 60%. The second stage of ageing at 480 °C did not affect the mechanical properties significantly. The same trend was observed for both Monel K500 and FM60 depositions; however, the absolute values of the strength and wear resistance varied. The comparison of as-weld depositions to the annealed hot-rolled plate and the corresponding age-hardening treatments has shown the hardness values of the wire-arc deposited Monel K500 to be very close to the corresponding hardness values of the Monel K500 plate. However, the strength of the plate was higher than this of the depositions for all studied heat treatment conditions. Thus, YS and UTS in the annealed Monel

K500 plate were 198–208 MPa and 294–316 MPa, respectively, higher than in the deposited Monel K500. After annealing and ageing at 610 °C, the YS and UTS were 215–265 MPa and 218–311 MPa, respectively, higher in the plate. Despite that, for all studied conditions, the wear resistance of the plate was on average twice as low (mass loss higher) as that of the depositions. This coincided with a 2–2.5 times lower elongation and up to 1.7 times lower toughness in the Monel K500 plate. In addition, the fracture of the Monel K500 plate was quasi-cleavage in contrast to the fully ductile fracture in the Monel K500 and FM60 depositions (Figure 11).

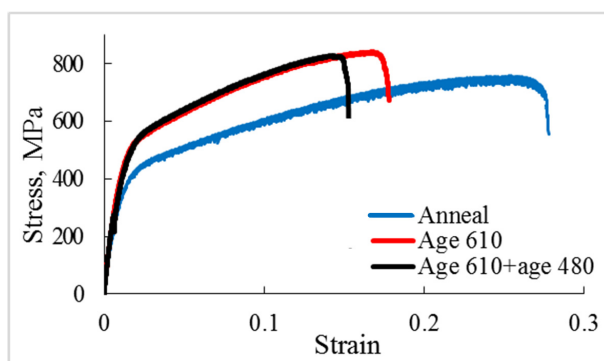


Figure 10. The tensile stress–strain curves of the Monel K500 plate.

Table 4. The mechanical properties of the Monel K500 plate.

Heat Treatment Condition	HV	YS, MPa	UTS, MPa	El, %	MPa·%	Mass Loss, g
Anneal	155	368	724 ± 20	25 ± 1	13,650	0.1821
Age at 610	250	515	833 ± 5	15 ± 1	10,110	0.1392
Age at 610 + 480	270	518	815 ± 10	12 ± 1	7998	0.1380

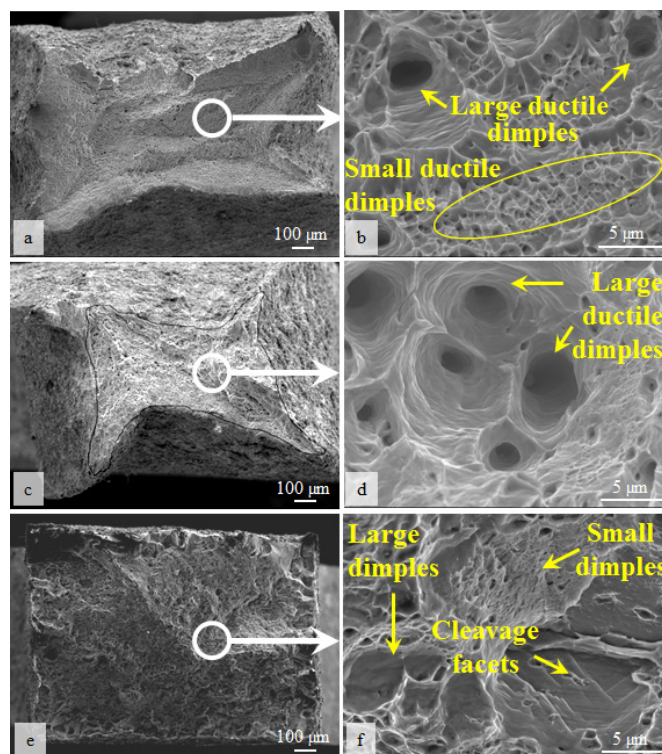


Figure 11. SEM images of the fracture surface in annealed and aged at 610 °C condition in (a,b) Monel K500, (c,d) FM60 and (e,f) Monel K500 plates.

4. Discussion

4.1. Effect of Alloy Composition and Processing on Grain Structure and Particle Parameters

Compared to FM60, Monel K500 wire contained several times lower Mn and Ti contents but higher Al and C contents. The higher C content has led to the precipitation of TiC/TiCN particles in Monel K500. However, in FM60, a higher Ti content did not lead to the precipitation of TiCN but rather to the precipitation of Ti-rich oxides. Ti-rich oxides were frequently observed in Ni-based alloys [14,15], in particular, in the core of TiN particles [16]. The latest indicates a possibility of Ti oxide precipitation at temperatures higher than TiCN. In our alloy FM60, this would mean a decrease in free Ti in solid solutions available for carbonitride precipitation after the Ti-rich oxides have precipitated.

In the as-weld condition, the number density of particles in both alloys decreased with an increase in deposition speed. This resulted from an increased cooling rate and decreased time available for precipitation with an increase in deposition speed. The number density of precipitates was 2 to 3 times (depending on deposition speed) higher in FM60 than in Monel K500. This mainly originated from a 4–7 times higher number density of Mn-rich particles in FM60, which corresponded to the 4 times higher Mn content in the FM60 composition. With an increase in deposition speed, the relative amount of Ti-rich particles decreased in both alloys (although to a greater extent in FM60). Faster cooling rates, due to higher deposition speeds, largely affected the precipitation of Ti-rich particles than the Mn-rich ones, as the precipitation temperatures of Ti oxides ($>1600\text{ }^{\circ}\text{C}$ [15]), nitrides ($>1200\text{ }^{\circ}\text{C}$ [16]) and carbide ($>1000\text{ }^{\circ}\text{C}$ [17,18]) are higher than those observed for Mn-rich particles (down to $800\text{ }^{\circ}\text{C}$ [19,20]).

After annealing and ageing at $610\text{ }^{\circ}\text{C}$, almost all the particles in Monel K500 were TiC/TiCN, and the particles number density dramatically (by 240–290 times) increased compared to the as-weld condition. It remains unclear whether the precipitation of Ti occurred during annealing or during subsequent ageing. For the Ti and C contents in Monel K500 (0.5 and 0.088 wt.%, respectively) and the solubility equation $\log [\text{Ti}] \cdot [\text{C}] = 2.75 - 7000/T$ presented in Reference [18], the temperature of full TiC dissolution could be about $1430\text{ }^{\circ}\text{C}$ in our Monel K500. This means that during annealing at $1100\text{ }^{\circ}\text{C}$, not dissolution but precipitation of TiC could take place. In FM60, the calculated dissolution temperature of TiC was lower ($1135\text{ }^{\circ}\text{C}$) than in Monel K500, although still a bit higher than the annealing temperature. However, precipitation of TiC in FM60 had to be slower not only because of the lower C content but also because of the higher Mn content. Mn was reported to increase solubility of Ti in face-centered cubic lattices [21,22]. A decrease in the relative amount of Mn-rich particles and increase in TiAl-rich ones in FM60 after annealing and ageing at $610\text{ }^{\circ}\text{C}$ could be due to the dissolution of some Mn-rich particles and the growth of fine TiAl-rich ones to the sizes large enough for observation in SEM. The variation in particle number density with deposition speed (namely, a decrease in number density with the speed increase) disappeared after annealing and ageing in Monel K500 and remained in FM60. Obviously, a significant variation in the particle chemistry, associated with the precipitation of TiC/TiCN in Monel K500 for all deposition speeds, altered this dependence.

During the second ageing at $480\text{ }^{\circ}\text{C}$, particle coarsening (Oswald ripening), accompanied by a decrease in number density, took place in both alloys. This phenomenon was observed previously in aged Ni alloys [23,24]. In addition, in FM60, either precipitation and growth of new Mn-rich particles or the growth of the Mn-rich shell on top of the Ti-rich core took place. This has led to the increase in the relative amount of Mn-rich particles in FM60 after the second ageing.

In the as-weld condition, the secondary dendrite arm spacing (SDAS) was in the same range of $4\text{--}12\text{ }\mu\text{m}$ in both alloys. This can be related to similar solidification and cooling conditions irrespective of the alloy composition. However, in Monel K500, SDAS decreased with an increase in deposition speed, and in FM60, no dependence of SDAS on deposition speed was observed. SEM visible Ti-rich particles, which could affect the grain growth rate during solidification, were of similar number density in both alloys and therefore, probably, did not play a significant role in the formation of the SDAS value. Particles smaller than 20 nm could be of varying density and might have influenced SDAS. However, these were not studied here and require further investigation using transmission electron

microscopy (TEM). During annealing and subsequent ageing, SDAS was growing in both alloys. However, the growth was larger in FM60 (up to 10–18 μm after the second ageing) compared to Monel K500 (up to 6–14 μm after the second ageing). Slower SDAS growth in Monel K500 can be explained by a much higher number density of TiC/TiCN particles pinning the dendrite boundaries and preventing their migration.

4.2. Effect Of Alloy Composition and Processing on Mechanical and Wear Properties

Due to the precipitation of TiC/TiCN particles and a smaller SDAS, Monel K500 exhibited higher hardness, YS and UTS than FM60 for all the studied conditions (Tables 2 and 3). In spite of the FM60 elongation being larger in annealed and aged conditions, the toughness of Monel K500 was higher due to higher strength. In accordance with higher hardness and toughness, the wear resistance of Monel K500 was higher in almost all the conditions (Figure 12).

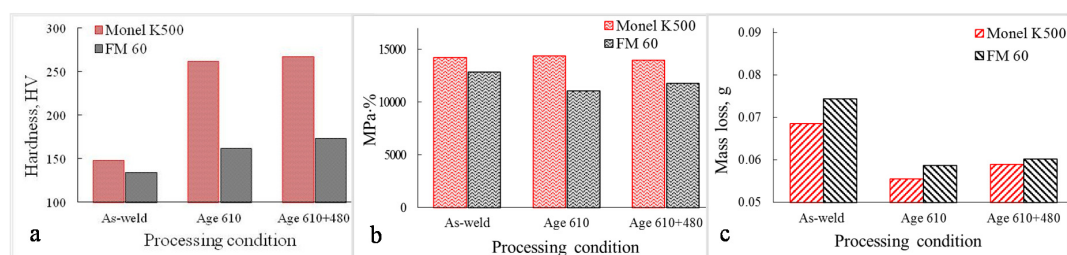


Figure 12. The variation in the mechanical properties, (a) hardness, (b) toughness and (c) wear resistance (mass loss), of Monel K500 (red) and FM60 (black) with heat treatment (500 mm/min deposition speed).

Annealing followed by ageing at 610 °C led to the hardness, strength and wear resistance increase in both alloys and toughness increase in Monel K500. These were due to the precipitation of Ti-rich particles in both alloys: TiC/TiCN in Monel K500 and Ti-rich oxides in FM60. However, a 240–290 times increase in the particle number density in Monel K500 seems to be disproportional to only a 16% increase in wear resistance, as only a 2 times increase in the particle number density in FM60 resulted in a 24% increase in wear resistance. Obviously, fine (<20 nm) particles not visible in SEM play a significant role in determining the mechanical properties in the studied alloys. These particles require a detailed investigation using TEM. Second ageing at 480 °C, following ageing at 610 °C, resulted in the particle growth accompanied by a decrease in the particle number density in both alloys. This could lead to either minor variations in hardness and strength or a noticeable decrease in those parameters in both alloys and a decrease in toughness in Monel K500. In spite of some increase in toughness in FM60, the wear resistance decreased in both alloys after the second ageing.

In the as-weld condition, the lowest hardness, strength and wear resistance in both alloys were observed for the slowest deposition speed of 300 mm/min. These coincided with the highest particle number density in both alloys. At slow deposition speeds, the cooling time is longer and particles have more time for precipitation in growth. While the large (SEM visible) particles are growing, the fine (TEM visible) particles may lose their number density, which would soften the matrix and reduce strength and wear resistance. In the annealed and aged conditions, the highest wear resistance (supported by either the highest hardness or strength) in both alloys was obtained at the highest deposition speed of 500 mm/min. These coincided with the low particle number density in the SEM visible particle size range (>20 nm). The role of <20 nm particles requires further investigation.

On the basis of this discussion, for future practical applications of wire deposited Ni–Cu alloys, we would recommend avoiding the second ageing heat treatment and applying reasonably high speeds during wire-arc deposition.

5. Conclusions

The first-ever investigation of the effect of heat treatment on the microstructure, mechanical properties and wear resistance of Ni–Cu alloys processed using the wire arc additive manufacturing technology has resulted in the following conclusions:

1. In the as-weld condition, precipitation of TiC and TiCN particles was observed in Monel K500, the alloy with a higher C content, rather than in FM60, containing a higher Ti content. In FM60, the precipitation of Ti-rich oxides and MnS-core particles took place, which coincided with a higher Mn content in FM60.
2. Annealing at 1100 °C followed by ageing at 610 °C resulted in an extensive precipitation of TiC particles in Monel K500 (a 240–290 times increase in the TiC number density compared to the as-weld condition). However, in FM60, the particle precipitation was relatively sluggish (up to a 70% increase in the number density). The second ageing at 410 °C has led to the particle coarsening, accompanied by a decrease in the particle number density, in both alloys.
3. Due to the precipitation of TiC/TiCN particles and the smaller secondary dendrite arm spacing, Monel K500 exhibited higher hardness, yield stress and tensile strength than FM60 for all the studied conditions. In spite of the FM60 elongation being larger in annealed and aged conditions, the toughness of Monel K500 was higher due to higher strength. In accordance with higher hardness and toughness, the wear resistance of Monel K500 was higher in almost all conditions.
4. In the as-weld condition, the lowest hardness, strength and wear resistance in both alloys were observed for the slowest deposition speed of 300 mm/min. These coincided with the highest particle number density in both alloys. In the annealed and aged conditions, the highest wear resistance (supported by either the highest hardness or strength) in both alloys was obtained at the highest deposition speed of 500 mm/min. These coincided with the low particle number density. In spite of a 240–290 times increase in the particle number density in Monel K500, after annealing and ageing at 610 °C, the wear resistance increased by only 16%, and only a 70% increase in the particle number density in FM60 resulted in a 24% increase in the wear resistance. Obviously, fine (<20 nm) particles, not visible in SEM and not studied here, played their role in properties development. This requires further investigation.

Author Contributions: O.M. has conducted the microstructure characterisation, mechanical property testing and analysis of the microstructure-properties relationship and has written the paper. A.K. assisted with microscopy experiments and contributed to the analysis of microstructure-properties relationship and paper writing. C.S. assisted with heat-treating the samples and tensile testing. Z.P., H.L. and S.v.D. carried out the overall project management and participated in the discussion of the results.

Acknowledgments: This project was financially supported by the Defence Materials Technology Centre (DMTC), which was established under the initiative of the Australian Government's Defence Future Capability Technology Centre (DFCTC). Olexandra Marenych is thankful for a scholarship sponsored by DMTC. The WAAM was carried out in the UOW Welding and Industrial Automation Research Centre. The assistance of Donghong Ding with samples preparation using WAAM is greatly appreciated. The JEOL JSM-7001F FEG-SEM used in this work for microstructure characterisation was funded by the Australian Research Council grant LE0882613.

Conflicts of Interest: The authors declare no conflict of interest.

References

1. High-Performance Alloys for Resistance to Aqueous corrosion, Special Metals Corporation, Publication number SMC-026. 2000. Available online: <https://www.scribd.com/document/55871734/Nickel-Base> (accessed on 12 December 2017).
2. Davis, J.R. *Nickel, Cobalt, and Their Alloys*; ASM International: Materials Park, OH, USA, 2000.
3. Bassford, T.H.; Hosier, J. Nickel and its Alloys. In *Handbook of Materials Selection*; Kutz, M., Ed.; Wiley: New York, NY, USA, 2002.
4. Lippold, J.C.; DuPont, J.N.; Kiser, S.D. *Welding Metallurgy and Weldability of Nickel-Base Alloys*; Wiley: New York, NY, USA, 2009.

5. Hibner, E.; Lemk, T.F. History of Monel Alloy K-500, Special Metals Corporation. 2002. Available online: <https://www.corrosionmaterials.com/k500-nickel-copper-alloy> (accessed on 12 December 2017).
6. Wu, B.; Ding, D.; Pan, Z.; Cuiuri, D.; Li, H.; Han, J.; Fei, Z. Effects of heat accumulation on the arc characteristics and metal transfer behavior in Wire Arc Additive Manufacturing of Ti6Al4V. *J. Mater. Process. Technol.* **2017**, *250*, 304–312. [[CrossRef](#)]
7. Wang, F.; Williams, S.; Rush, M. Morphology investigation on direct current pulsed gas tungsten arc welded additive layer manufactured Ti6Al4V alloy. *Int. J. Adv. Manuf. Technol.* **2011**, *57*, 597–603. [[CrossRef](#)]
8. Haden, C.; Zeng, G.; Carter, F.; Ruhl, C.; Krick, B.; Harlow, D. Wire and arc additive manufactured steel: tensile and wear properties. *Addit. Manuf.* **2017**, *16*, 115–123. [[CrossRef](#)]
9. Shen, C.; Pan, Z.; Cuiuri, D.; Ding, D.; Li, H. Influences of deposition current and interpass temperature to the Fe3Al-based iron aluminide fabricated using wire-arc additive manufacturing process. *Int. J. Adv. Manuf. Technol.* **2018**, *88*, 2009–2018. [[CrossRef](#)]
10. Cong, B.; Ding, J.; Williams, S. Effect of arc mode in cold metal transfer process on porosity of additively manufactured Al-6.3%Cu alloy. *Int. J. Adv. Manuf. Technol.* **2015**, *76*, 1593–1606. [[CrossRef](#)]
11. Ding, D.; Pan, Z.; Van Duin, S.; Li, H.; Shen, C. Fabricating superior NiAl Bronze components through wire arc additive manufacturing. *Materials* **2016**, *9*, 652. [[CrossRef](#)] [[PubMed](#)]
12. Xu, F.; Lv, Y.; Xu, B.; Liu, Y.; Shu, F.; He, P. Effect of deposition strategy on the microstructure and mechanical properties of Inconel 625 superalloy fabricated by pulsed plasma arc deposition. *Mater. Des.* **2013**, *45*, 446–455. [[CrossRef](#)]
13. Baufeld, B. Mechanical properties of Inconel 718 parts manufactured by shaped metal deposition (SMD). *J. Mater. Eng. Perform.* **2012**, *21*, 1416–1421. [[CrossRef](#)]
14. Lim, Y.S.; Kim, H.P.; Jung, M.K.; Kim, J.S. Phase analysis of the precipitates in an Alloy 600/182 weld. *Solid State Phenom.* **2007**, *119*, 111–114. [[CrossRef](#)]
15. Dashevskii, V.Y.; Aleksandrov, A.; Kanevskii, A.G.; Makarov, M.A. Deoxidation Equilibrium of Titanium in the Iron–Nickel Melts. *ISIJ Int.* **2010**, *50*, 44–52. [[CrossRef](#)]
16. Karasev, A.V.; Suito, H. Nitride precipitation on particles in Fe–10mass%Ni alloy deoxidized with Ti, M (M_Mg, Zr and Ce) and Ti/M. *ISIJ Int.* **2009**, *49*, 229–238. [[CrossRef](#)]
17. Soto, R.; Saikaly, W.; Bano, X.; Issartel, C.; Rigaut, G.; Charai, A. Statistical and theoretical analysis of precipitates in dual-phase steels microalloyed with titanium and their effect on mechanical properties. *Acta Mater.* **1999**, *47*, 3475–3481. [[CrossRef](#)]
18. Strid, J.; Easterling, K.E. On the chemistry and stability of complex carbides and nitrides in microalloyed steels. *Acta Metall.* **1985**, *33*, 2057–2074. [[CrossRef](#)]
19. Chen, Y.; Wang, Y.; Zhao, A. Precipitation of AlN and MnS in low carbon aluminium killed steel. *J. Iron Steel Res. Int.* **2012**, *19*, 51–56. [[CrossRef](#)]
20. Garbarz, B.; Marcisz, J.; Wojtas, J. TEM analysis of fine sulphides dissolution and precipitation in steel. *Mater. Chem. Phys.* **2003**, *81*, 486–489. [[CrossRef](#)]
21. Akben, M.; Chandra, T.; Plassiard, P.; Jonas, J. Dynamic precipitation and solute hardening in a titanium microalloyed steel containing three levels of manganese. *Acta Metall.* **1984**, *32*, 591–601. [[CrossRef](#)]
22. Wang, Z.; Sun, X.; Yang, Z.; Yong, Q.; Zhang, C.; Li, Z.; Weng, Y. Effect of Mn concentration on the kinetics of strain induced precipitation in Ti microalloyed steels. *Mater. Sci. Eng. A* **2013**, *561*, 212–219. [[CrossRef](#)]
23. Angella, G.; Donnini, R.; Ripamonti, D.; Maldini, M. The role of particle ripening on the creep acceleration of Nimonic 263 superalloy. *MATEC Web Conf.* **2014**, *14*, 14001. [[CrossRef](#)]
24. Baldan, A. Review: Progress in Ostwald ripening theories and their applications to the γ' -precipitates in nickel-base superalloys, Part II Nickel-base superalloys. *J. Mater. Sci.* **2002**, *37*, 2379–2405. [[CrossRef](#)]

